Article

Limited Crystallite Growth upon Isothermal Annealing of Nanocrystalline Anatase

Davide Casotti, Matteo Ardit, Robert E. Dinnebier, Michele Dondi, Francesco Matteucci, Isabella Zama, and Giuseppe Cruciani

Cryst. Growth Des., **Just Accepted Manuscript** • DOI: 10.1021/acs.cgd.5b00068 • Publication Date (Web): 10 Apr 2015

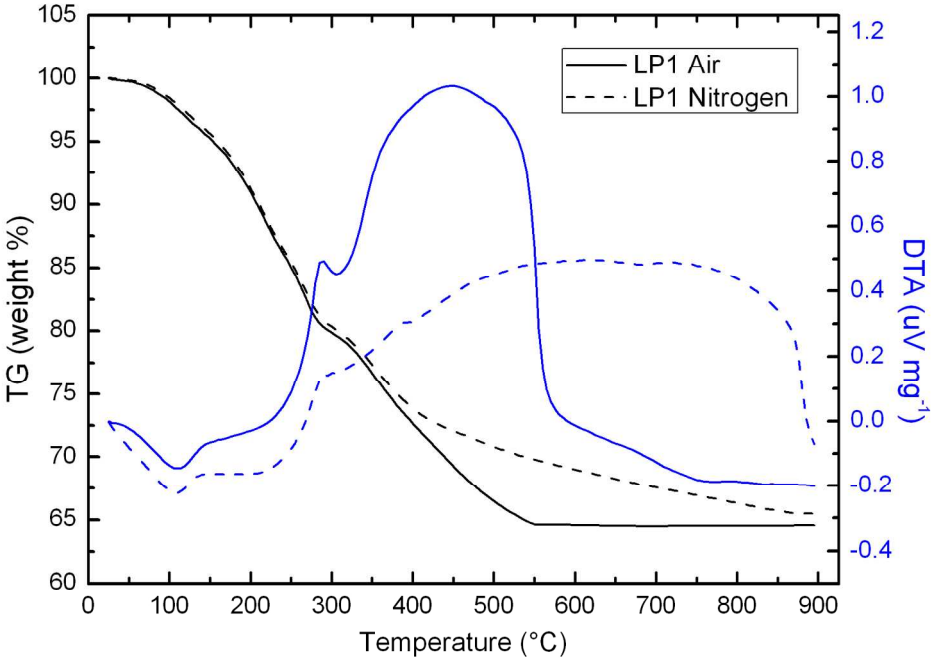

499x364mm (96 x 96 DPI)

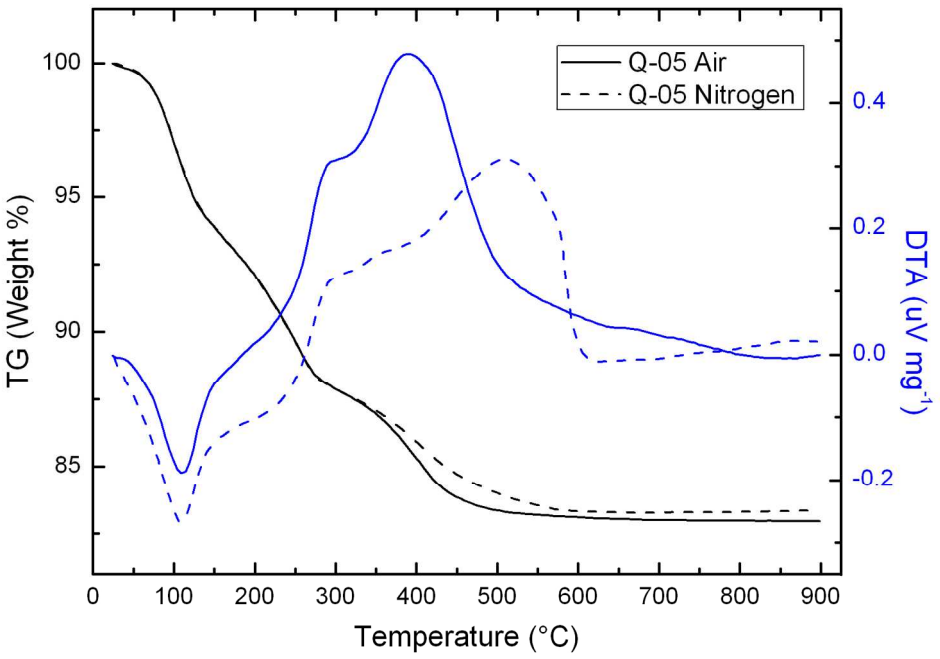

499x357mm (96 x 96 DPI)

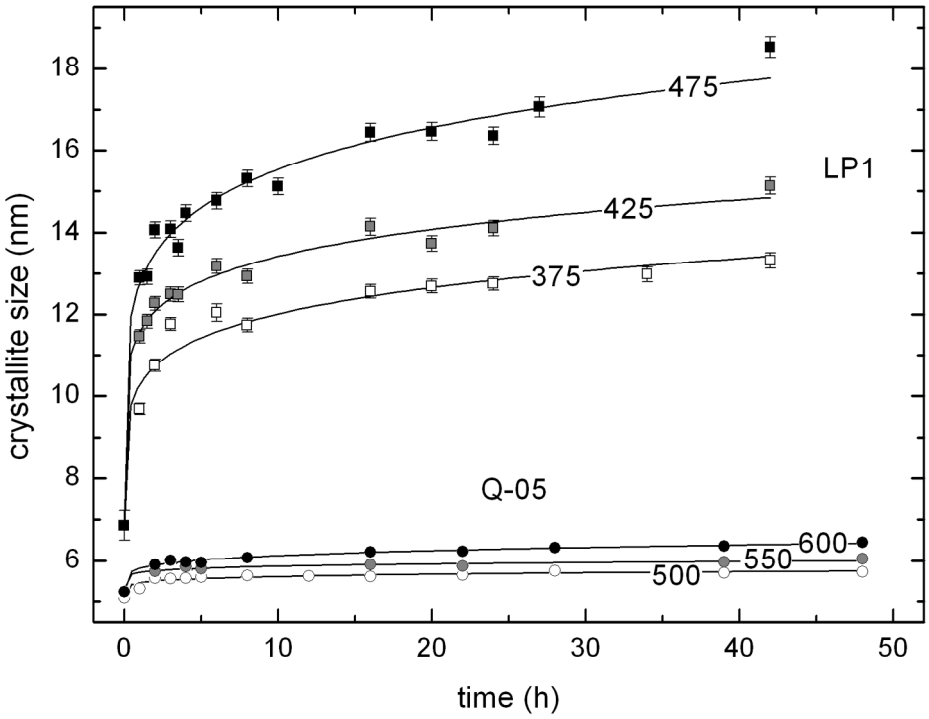

499x392mm (96 x 96 DPI)

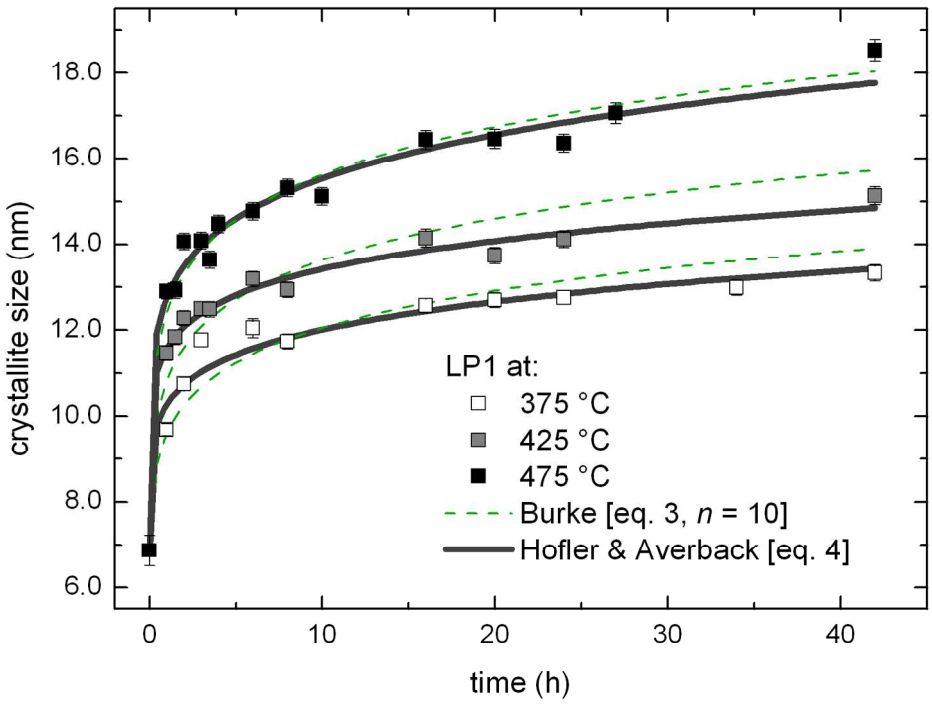

499x384mm (96 x 96 DPI)

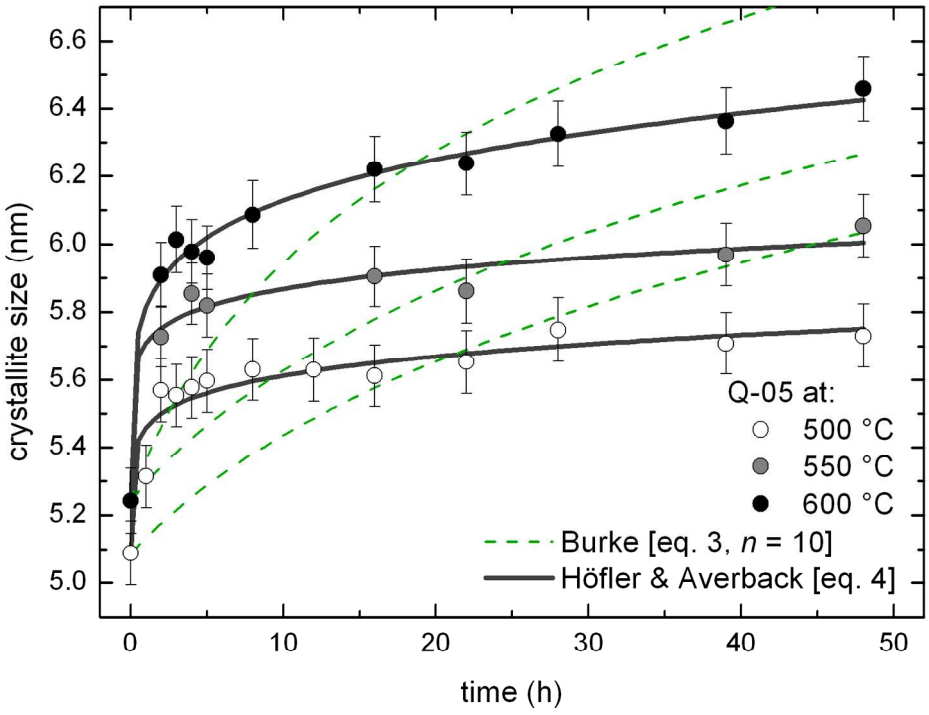

499x389mm (96 x 96 DPI)

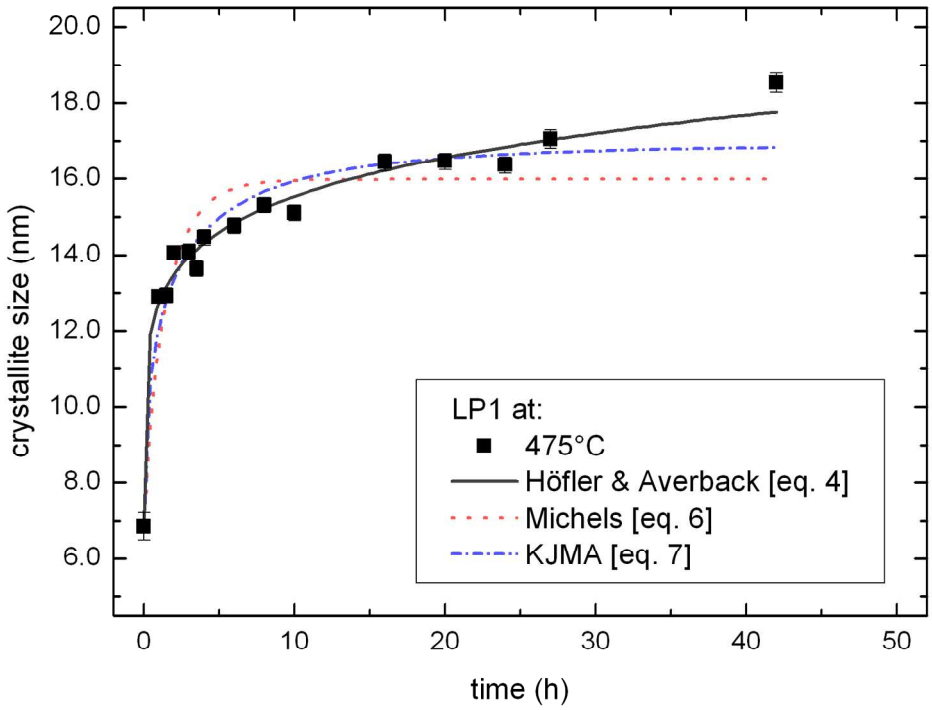

499x387mm (96 x 96 DPI)

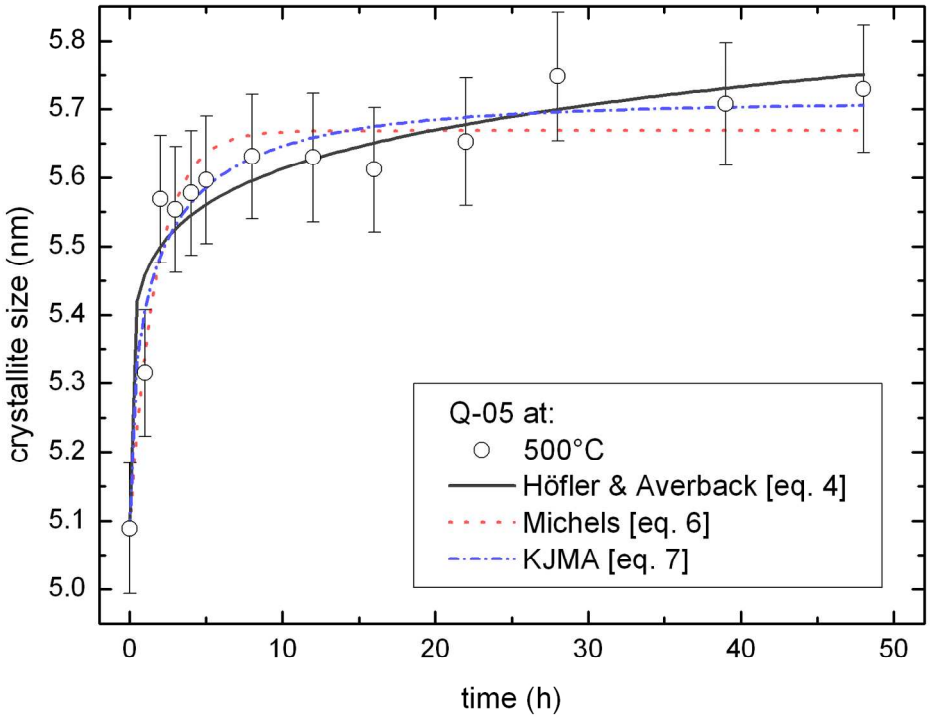

499x392mm (96 x 96 DPI)

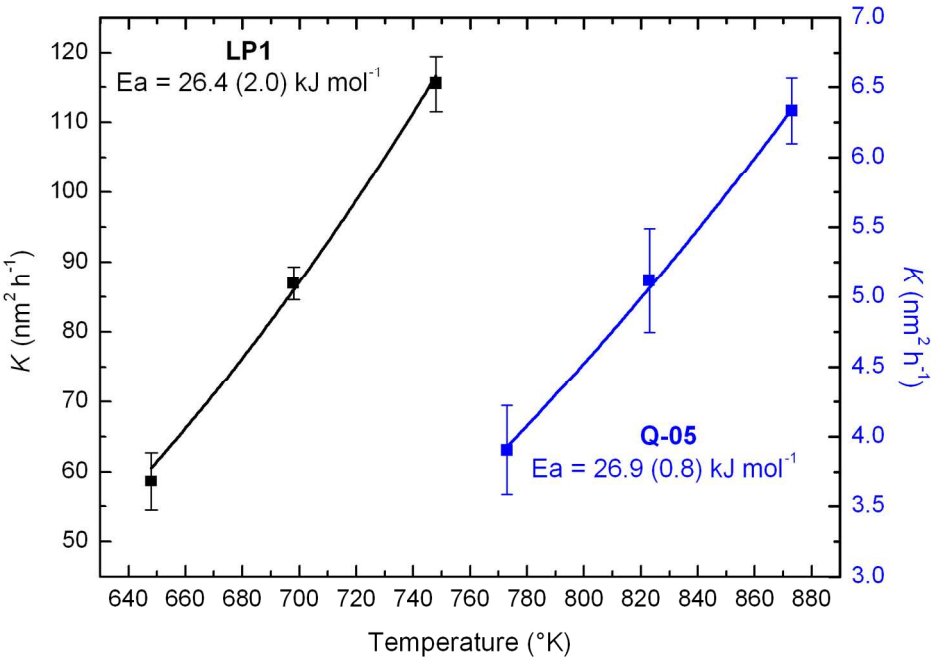

499x363mm (96 x 96 DPI)

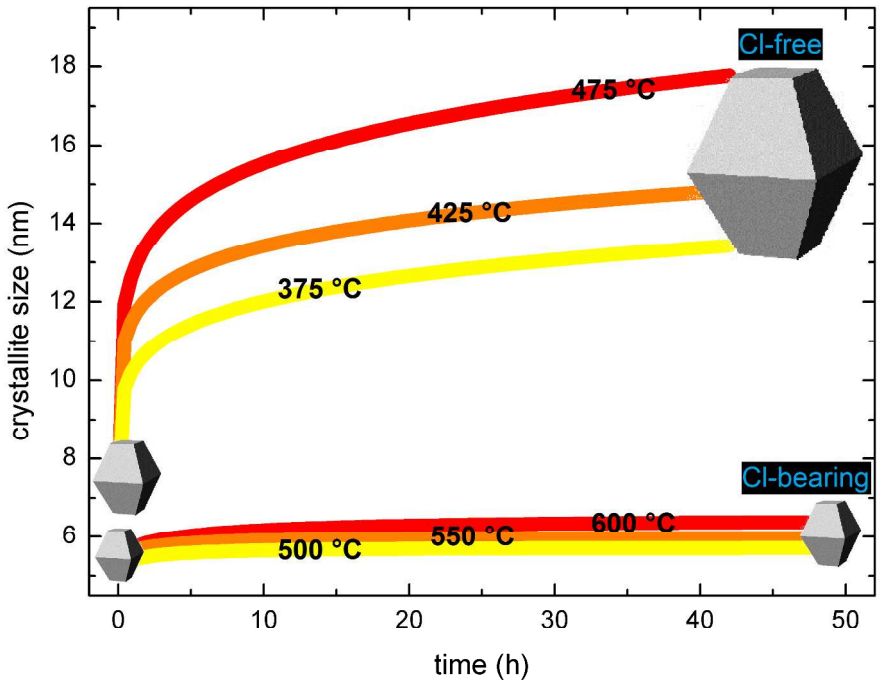

912x697mm (96 x 96 DPI)

Limited Crystallite Growth upon Isothermal Annealing of Nanocrystalline Anatase

Davide Casotti,[a,b] Matteo Ardit,[a] Robert Dinnebier,[c] Michele Dondi,[d] Francesco Matteucci,[e] Isabella Zama,[f] and Giuseppe Cruciani,[*,a]

[a] Department of Physics and Earth Sciences, University of Ferrara, Italy
[b] Department of Physics, Informatics and Mathematics, University of Modena and Reggio Emilia, Modena, Italy
[c] Max-Plank Institute for Solid State Research, Stuttgart, Germany
[d] Institute of Science and Technology for Ceramics, CNR-ISTEC Faenza, Italy
[e] Nanotechnology Living Lab (NTLL) at Dhitech, Lecce, Italy
[f] Tozzi Renewable Energy, Ravenna, Italy

ABSTRACT The crystalline growth kinetics during isothermal sintering of two nanotitania powders synthesized by similar routes, but with and without the presence of chlorine in the synthesis batch) were studied by X-ray powder diffraction and modelled by several grain growth models. Both nanopowders contained anatase as the initial titania phase with similar crystallite dimension. Crystal growth curves at three isotherms per each samples were sampled over a period of time up to 40 h. Temperature steps within different ranges (375, 425, and 475 °C for Cl-free sample; 500, 550, and 600 °C for Cl-containing sample) were chosen. The XRD analysis of samples heated at 900°C revealed that, while the entire Cl-free sample was converted to rutile, only 10% of the Cl-containing sample had transformed to rutile with a very limited crystal growth. Direct comparison of the crystal growth curves show different behaviour which was modelled by different grain growth kinetic equations which include a growth limiting factor. Although the generalized parabolic grain growth model with time-exponent (so called "Höfler-Averback equation") provided good fits for both the Cl-free and Cl-containing nanopowders at all temperature, only the isothermal curve at 500°C of the Cl-containing sample was satisfactorily fitted with a modified KJMA equation. The activation energy of the grain growth are very similar and in line with the previously reported values. We conclude that the crystal size locking phenomenon observed for Cl-bearing anatase can be ascribed to the effects of chlorine ions adsorbed on grain surface as previously suggested. The blocked crystal growth of nanoanatase obtained by the reflux synthesis of organic solvents in the presence of hydrochloric acid as catalyst makes this material very appealing for devices that require a given nanosize and for anatase phase in spite of the high temperature processing.

INTRODUCTION

Titanium dioxide (TiO_2) is a deeply investigated material that finds several applications as technological material, such as: pollutant elimination through photocatalysis,[1] mechanical and anti-corrosion application,[2] selective reduction of NO_x,[3] organic compounds synthesis,[4] white pigment in paints,[5] additive in food, pharmaceuticals and cosmetics,[6] potential tool in cancer treatment,[7] sensors,[8] and as a component of photovoltaic electrochemical cells.[9]

Among photovoltaic devices, the so-called Dye-Sensitized Solar Cells (DSSC)[10,11] or Grätzel's cells have received particular attention being considered one of the new alternative sources of energy as a supplement to the fossil fuels and to replace the traditional and more expensive silicon cells,[12] and integrated in the glass windows of buildings.[13] In the last decade, many works have been devoted to improve every single component of DSSC devices by exploring new electrolytes,[14,15] dyes,[16,17] cell architectures,[18,19] and electrodes.[20–22] More recently, the traditional organic dye sensitizer has been replaced by highly efficiency perovskite sensitizer, keeping the traditional nanostructured anatase electrode.[23,24]

A paste obtained by dispersing nano-TiO_2 in a suitable organic medium is typically applied on a conductive glass by screen printing or doctor blade method,[25–27] then the electrode undergoes an annealing cycle in order to remove the organic components and sinter the titania film on the glassy substrate. The result is a thin layer (~10 μm thick)[10,11] of nano-anatase characterized by open pores.[20] The driving force of sintering tends to reduce the surface energy of the anatase nanocrystals, producing a growth of the particle size and an increase of the bulk density.[28,29] This phenomenon leads to a substantial reduction of transparency,[30] as well as performances of DSSC devices; hence, it should be prevented or strongly contrasted.[10,11,20] A brief description of processes operating during the sintering of nano-powder will be given in the next paragraph.
This work is aimed at investigating the crystal growth kinetics of nanocrystalline anatase powders under isothermal sintering. X-ray powder diffraction (XRPD) and thermal analyses (TG/DTA) were used to monitor the annealing behaviour of two powder samples obtained through the same synthesis route but differing for the catalyst and solvent present in the batch. In order to investigate the distinct nanocrystal growth of the two samples, several grain growth kinetic models are reviewed and tested by fitting the isothermal annealing curves.

THEORETICAL BACKGROUND

Several studies have been devoted to investigate the sintering processes on both "ideal" (theoretical) and "real" nano-powders. Ideal powders are assumed as composed by crystals perfectly spherical having the same diameter,[28,31] whereas real powders are characterized by particles that do not have neither an ideal shape nor the same diameter and are usually organized as aggregates.[29,32–35]
During the sintering processes both ideal and real powders change their microstructural properties through three stages of evolution where necks between particles, open pores and closed pores are the dominating features, respectively.[28,29,31] According to classical sintering theories, ideal powders in the first and in the second stage of sintering, (when relative density as whole is lower than 90%,) are characterized by an interparticle diffusion mechanism that acts by creating necks between particles, so making powders denser and cohesive.[28,29,31] While in the first stage of sintering only the neck growth mechanism is active, during the second stage, particularly on real powders, densification, neck growth and grain growth operate simultaneously.[28,29,31,36,37] During the final stage of sintering (when relative density > 90%) the pores are closed by diffusion mechanisms, and a grain coarsening takes place by means of a grain boundary migration.[28,29,31,38]
The behaviour of nanoparticles during the sintering process can be rationalized in both thermodynamic and kinetic terms. In its generalized form, the thermodynamic driving force of sintering (σ) is written as:

$$\sigma = \gamma\theta = \gamma\left(\frac{1}{r_1} + \frac{1}{r_2}\right) \qquad (1)$$

where γ is the specific surface energy of the particles, θ is the curvature of particle surfaces, and r_1 and r_2 are the radii of curvature of the surfaces. From equation 1 stems out that the driving force for particles growth is inversely related to their size and directly proportional to their surface energy.[28,29,39–41]
The first theoretical considerations on the grain growth kinetics were developed by Beck,[42] Burke,[39] and Burke and Turnbull.[43] This theory, known as the *classical parabolic grain growth model* or more simply as the *Burke's equation*, is based on the assumption that the crystallite growth kinetic should ideally follow a parabolic curve, where the rate of the crystallite growth is inversely related to the particle size.[29,38,39,40,44–48] This equation has the form:[46]

$$\frac{dR}{dt} = \frac{K}{R} \Rightarrow R_t^2 - R_0^2 = 2Kt \quad (2)$$

where K is a temperature and material dependent rate constant, R_t is the mean crystallite diameter at time t of the sintering process, and R_0 is the initial crystallite diameter at $t = 0$.[38,47] In the case of $R_t >> R_0$, R_0 can be disregarded, e.g. when the starting material is an amorphous phase.[40,44,48] Since equation 2 was found to not properly reproduce all the experimental data sets,[29,38,44–49] the *classical parabolic grain growth model* was reformulated in the form of a *generalized parabolic grain growth model*:[46]

$$R_t^n - R_0^n = nKt \quad (3)$$

where n is an empirical grain growth exponent, that generally varies between 2 and 4.[38,46–49] The exponent n of the values R_t and R_0 is usually related to mechanisms of grain growth as will be discussed in detail in the next section. Curve fitting to equation 3 with nanocrystalline materials can lead to an exponent n higher than 10 which is considered the highest realistic and physically meaningful value.[47]

In order to overcome deviations from ideality, during a study of sintering on nanorutile powders, Höfler and Averback introduced a time-dependent exponent, m, in the Burke's equation by keeping constant the size-dependent exponent (i.e. $n = 2$):[50]

$$R_t^2 - R_0^2 = 2Kt^m \quad (4)$$

The same authors stated that, as in the case of the size-dependent exponent, the time exponent (m) could be affected by the same factors considered in the generalized parabolic grain growth model (eq. 3) namely, the pinning of grain boundaries by inclusions or pores and solute drag on the boundaries.[50] The Höfler-Averback's model has been successfully applied in isothermal sintering studies on both anatase and rutile.[50–52]

All of the above-mentioned models predict that grain growth is maintained even for long sintering times. However, the grain growth process might be blocked for prolonged sintering. This locking effect can be also related, besides the factors affecting the time-exponent (previously listed in order to explain the equation 4) to the small sample thickness.[29, 38,45,46]

For these reasons, equation 2 has been further modified by Burke by taking into account the locking effects through a *grain growth model with impediment*:[39,46]

$$\frac{R_0 - R_t}{R_{\max}} + \ln\left(\frac{R_{\max} - R_0}{R_{\max} - R_t}\right) = \frac{K}{R_{\max}^2}t \quad (5)$$

where $R_{\max}$ is the maximum average grain-size reached during the grain growth. Through this equation, it is assumed that the grain pinning effect is independent from the grain-size R. In the case of a dependence between grain-growth and grain-size (e.g. solute on boundaries) a different approach should be followed. As proposed by Michels et al.,[46] it seems reasonable to connect the concentration of surface impurities with the particle size (R).[29,38,46,47] This hypothesis finds its application in *the grain growth model with size dependent impediment*:[46]

$$R_t = \left[R_{\max}^2 - \left(R_{\max}^2 - R_0^2\right)\exp\left(-\frac{2Kt}{R_{\max}^2}\right)\right]^{1/2} \quad (6)$$

On the other hand, Michels et. al. have demonstrated that the application of the equations 5 and 6 leads to very similar results.[46]

In a recent review on the kinetic models for aggregative nanocrystal growth,[53] Wang et al. have pointed out that a modified Kolmogorov–Johnson–Mehl–Avrami (KJMA) expression is suitable to fit the sigmoidal profile of the limited crystal growth, in spite of its major drawback due to the lack of precise physical meaning for the rate parameters (K) and the Avrami exponent (n). Although the KJMA model can be rigorously applied to specific types of solid-state phase transformations, it has also been used to fit other nucleation and growth processes exhibiting sigmoidal conversion kinetics. We therefore also considered the following KJMA equation:

$$\frac{R_t^3}{R_{\max}^3} = \frac{R_0^3}{R_{\max}^3} + \left(1 - \frac{R_0^3}{R_{\max}^3}\right)\left[1 - \exp\left(-Kt^{\alpha}\right)\right] \quad (7)$$

where R_t is the nanocrystal mean diameter at time t, $R_{\max}$ is the nanocrystal mean diameter and R_0 is the primary nanocrystal mean diameter. A rate parameter (K) and the Avrami exponent (α) are the two fitting parameters in equation 7. For solid-state phase transformations, the value of α is often related to the mechanism of nucleation and the dimensionality of growth and it usually varies between 0.5 and 4.[54]

EXPERIMENTAL METHODS

Synthesis of anatase nano-powders. The investigated nano-powders, labelled as LP1 and Q-05, were produced according to a synthesis method patented by Daunia Solar Cell.[55,56] Both nano-powders were obtained by reflux synthesis of organic solvents starting from titanium tetraisopropoxide, $Ti(OC_3H_7)_4$ (*TTIP*), as common precursor. The main difference between the two synthesis routes consists in the composition of solvents and catalysts, being respectively benzyl alcohol (C_7H_8O) and acetic acid ($C_2H_4O_2$) for LP1; isobutyl acetate ($C_6H_{12}O_2$) and hydrochloric acid (HCl) for Q-05 (details on the synthesis procedure are given in the two patents).[55,56] Powders were obtained by spray drying of as-synthesized suspensions.

Annealing. Isothermal runs were carried out in an electric furnace in static air. Several sample aliquots are placed into unsealed ceramic crucibles. The firing schedule consisted of an initial heating ramp (30 minutes for LP1 and 60 minutes for Q-05) to reach a selected plateau temperature. Selected isotherms were at 375, 425, 475 °C for LP1 and 500, 550, 600 °C for Q-05. Samples were kept at each isotherm up to 40 h for LP1 and 48 h for Q-05 while aliquots were taken out at pre-set time intervals and naturally cooled down to room temperature before X-ray measurements. Different isotherm ranges for Q-05 (500–600 °C) and LP-1 (375–475 °C) have been chosen because Q-05 did not exhibit any crystal growth at lower temperatures.

TG/DTA analysis. The characterization of synthesis residues on the as synthesized powders was performed by simultaneous TG/DTA analysis using a Netzsch 409 PC Luxx thermal analyzer, with α-Al_2O_3 as reference for DTA. About 70 mg of samples were analyzed in the 20–900 °C range, with heating rate of 10 °C·min^{-1} under air and nitrogen flow of 20 ml·h^{-1}. The powders residues have been analysed by XRD.

Powder diffraction measurements. X-ray data collections of powder residues after thermal analyses and samples heated at different time-steps during the isothermal runs were performed at room temperature on a Bruker D8 Advance diffractometer with an X-ray tube operating at 40 kV and 40 mA, and equipped with a Si(Li) solid-state detector (SOL-X) set to discriminate the Cu$K\alpha_{1,2}$ radiation. Sample were mounted on a quartz zero-background holder or side-loaded on an aluminium holder. Measuring conditions were 5 to 75 °2θ range, 0.02 °2θ scan rate, and 2 s per step of counting time.

XRPD interpretation. Quantitative phase analysis and crystallite size/shape evaluation were performed by the Rietveld method as implemented in the TOPAS v.4 program by Bruker AXS.[57] The fundamental parameters approach was used for the line-profile fitting.[58–60] The determination of crystallite size by TOPAS was accomplished by the Double-Voigt approach.[61] In particular, the crystallite size was calculated as volume-weighted for the mean column heights based on integral breadths of peaks. The average crystallite size of anatase was obtained by profile fitting of the full 2θ range (i.e. through the Pawley's method) while the anisotropy of crystallite dimensions (i.e. the crystallite size of anatase along [001]) was determined by separately fitting the (004) and (015) anatase lines. The ratio between average crystallite size and the corresponding value along the *c*-axis provided a direct and simple index to estimate the average crystallite shape (aspect ratio) of each sample.

RESULTS

Thermal analyses (TG/DTA). TG analyses on the as synthesized powders reveal distinct behaviours (see Figure 1). The total weight loss at 900 °C is about 35% for LP1 and 18% for Q-05, regardless of the atmosphere used during the analysis (i.e. air and nitrogen). In spite of this large difference, the TG and DTA curves of both samples show similar trends encompassing three distinct steps in the following temperature ranges:

a) 50–150 °C. Weight losses of ~4% at 130°C in LP1 and ~6% at 150°C in Q-05, associated to a well defined endothermic reaction and unaffected by the used atmosphere, can be attributed to removal of all adsorbed water and of the more weakly bound solvents;

b) 150–280 °C. Weight losses (~15% for LP1 and ~6% for Q-05) occurring in this temperature range have a prevalent endothermic character which is partly overlapped with the exothermic reactions dominating in the next temperature range. Evaporation of the largest fraction of more tightly bound solvent residues explains this endothermic regime. The higher boiling point temperature of benzyl alcohol (205 °C) compared to isobutyl acetate (117 °C) explains the larger solvent fraction released by LP1 within this intermediate *T*-range compared to Q-05, whose solvent loss is relatively larger in the lower *T*-range;

c) 280–550 °C. Although to a different extent (~16% for LP1 and 5% for Q-05), the largest weight loss for both samples occurs in this *T*-range, and corresponds to a pronounced exothermal reaction which is broader and shifted to higher temperatures when the analysis is carried out in nitrogen atmosphere (especially in the case of LP1).

These features are characteristic of a combustion reaction, connected to solvent residues (self-ignition point: ~436 °C and ~422 °C for benzyl alcohol and isobutyl acetate, respectively) and their decomposition in by-products.

These observations imply that this combustion reaction occurred during the experiments of crystallite growth of nanoanatase LP1 (375–475 °C) but it was already over in the case of Q-05 (500–600 °C).

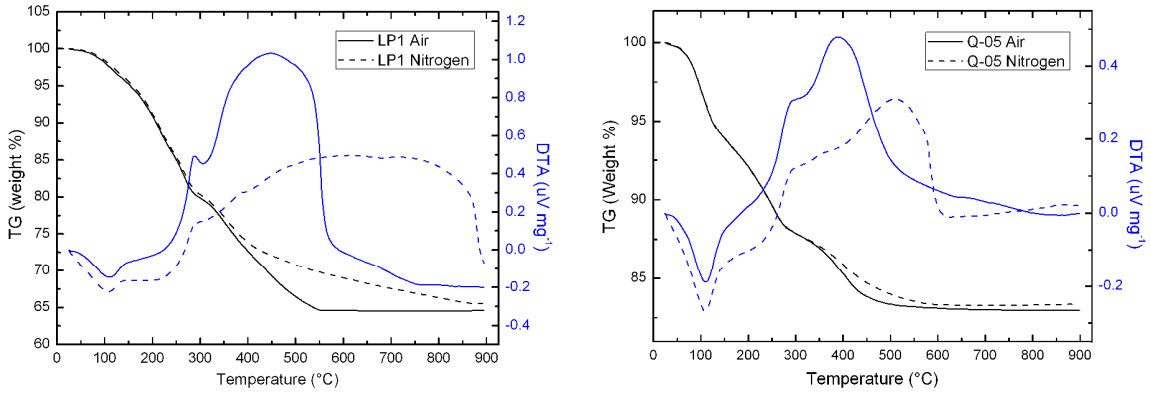

Figure 1. TG (left axis, black lines) and DTA (right axis, blue lines) analysis of samples LP1 (on the left) and Q-05 (on the right). Solid and dashed lines represent air and nitrogen atmospheres, respectively.

XRD analyses. Powder XRD patterns collected on the as-synthesized materials reveal that TiO_2 is present in both LP1 and Q-05 samples with the anatase structure (tetragonal, s.g. $I4_1/amd$), no other crystalline phases are detected. The average crystallite size for the as synthesized samples is 6.9 ± 0.4 nm (LP1) and 5.2 ± 0.1 nm (Q-05). In both cases, crystals are rod-like with an aspect ratio of about 2.6 and 2.9 for LP1 and Q-05, respectively. Upon thermal treatments (see below), for both samples the aspect ratio decreased in the initial stage then remained constant over the annealing time.

Powder XRD analyses on samples recovered after TG/DTA runs show that LP1 undergoes a complete transformation to rutile polymorph in both air and nitrogen, whereas Q-05 preserves about 90% of the initial anatase structure (i.e. only ~10% transforms to rutile) by maintaining a very small crystallite size (i.e. ~9.5 nm) even after thermal treatment at 900 °C.

XRD patterns collected on sample aliquots taken at selected intervals during the isothermal annealing process show that no anatase-to- rutile phase transition or appearance of new phases occur in the thermal ranges under investigation (375–475 °C for LP1 and 500–600 °C for Q-05). In both samples anatase undergoes a crystallite size growth, but two clearly distinct trends characterize the samples LP1 and Q-05 as a function of time (Figure 2).

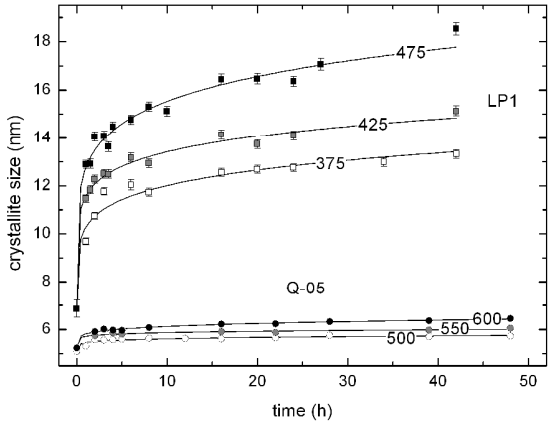

Figure 2. LP1 and Q-05 crystallite growth vs. isothermal annealing time. Error bars, where not shown, are within the symbol size. Lines are guide to the eye (with temperature in °C).

The crystallite growth of the sample LP1 is pronounced during the first hour of annealing (when the initial crystallite size is doubled). Thereafter, the rate of growth is progressively reduced, though a gradual increasing of crystallite size is still ongoing after 42 hours. This trend is in agreement to

what already observed for other anatase nanopowders.[34,51,52] Although heated at higher temperatures, the sample Q-05 undergoes just a very small crystallite size increasing during the first hour of treatment (when the size turns ~1.15 times that of the starting powder) and the rate is even lower after this earlier stage. This behaviour suggests that the coarsening of sample Q-05 is constrained by a growth-limiting effect and the nanosize increase is blocked even at higher temperatures (up to 900°C) hindering the anatase-to-rutile transformation.

Fitting the nanocrystal growth. As outlined in the "theoretical background", the growth of nanoparticles during annealing can be described by means of different kinetic models, some including an impediment factor. Among the refinable variables, the different expressions contain a rate parameter (here K), a dimension-exponent (here n), and a time-exponent (here m or the Avrami, α); some also include an upper limit size.

In order to define the best fitting model of growth kinetics for both LP1 and Q-05 samples, each isothermal curve was processed by OriginPro v.8 data analysis software by comparing several nonlinear curve regressions (equations from 2 to 7).[62] The goodness of fit for each curve regression is listed in Table 1 for a few selected equations by considering two indexes: (i) the adjusted r-square, R^2, and (ii) the reduced chi-square, χ^2, meaning that the degrees of freedom (i.e. number of data points and number of parameters) of the minimized equation are taken into account.

Initial fits based on the *classic parabolic grain growth model* (equation 2) do not converge while those based on its *generalised form* (equation 3) yield unreasonably high values of the grain growth exponent n (data not reported in Table 1). When in equation 3 n is kept fixed to 10, i.e. the highest physically-acceptable value,[47] fits converge to relatively poor agreement factors for LP1 while still diverge for Q-05 (see Figure 3). Fully satisfactory fits are achieved using the Höfler and Averback equation of growth (eq. 4). The refined time-dependent exponent, m, ranges from 0.13 to 0.23, an interval which is close to that reported for similar materials.[52]

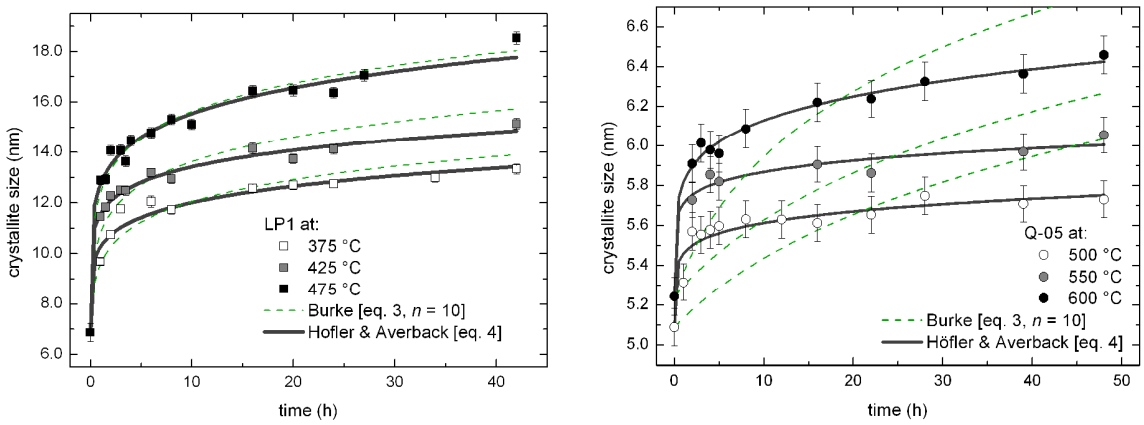

Figure 3. Mean crystallite size *vs.* isothermal annealing time (LP1 and Q-05 on the left and on the right side, respectively). Comparison of curve fittings by means of two different equations of growth: Höfler and Averback (*solid lines*)[50] and Burke (generalized parabolic grain growth model)[46] with grain growth exponent $n = 10$ (*dashes*).

In order to emphasize the different crystal growth regime of LP1 and Q-05, the nearest isotherms are considered (i.e. 475°C and 500°C, respectively) and the growth curves are also modelled using expressions which include a growth locking factor (see Figure 4).

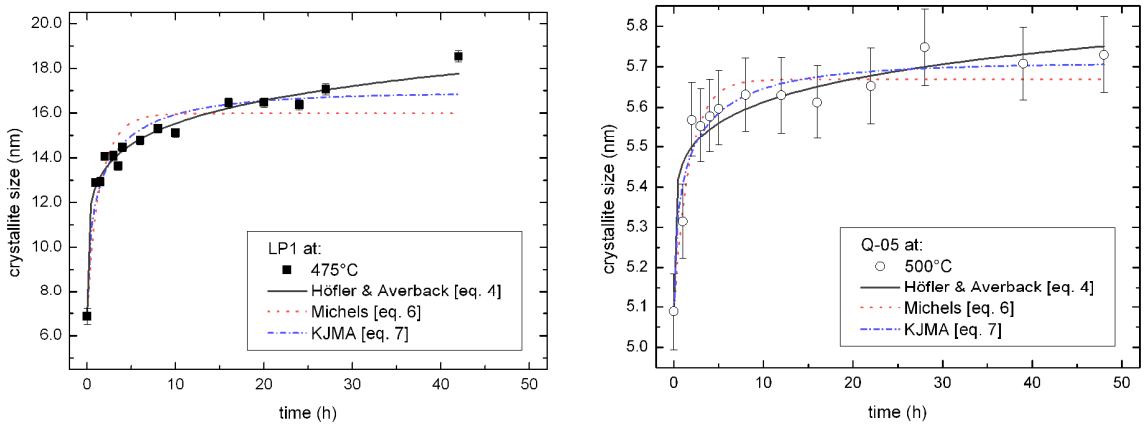

Figure 4. Isothermal annealing curves for LP1 at 475°C (*left*) and Q-05 at 500°C (*right*). Comparison of curve fittings by means of three different equations of growth: Höfler and Averback (*solid lines*),[50] Michels (*dotted line*),[46] and KJMA (*dash-dot line*).

Michel's equation 6, based on the *grain growth with impediment* model, yields unreasonable fits for the sample LP1 at 475°C, while acceptable fits are obtained for Q-05 at 500°C. The equation 6 has been shown to provide results very similar to equation 5.[46]

A significantly better fit, with a quality as good as the fit by the Höfler and Averback equation, is achieved when the Q-05 annealing curve at 500°C is modelled using the modified KJMA expression (eq. 7). The fitting parameters refined for Q-05 with the KJMA model are physically sound; in particular the α exponent, which fluctuates around 0.5, is in line with previously reported values.[54] In contrast, results of KJMA fitting of LP1 at 475°C are unsatisfactory and physically inconsistent (cfr. Fig. 4). Thus, the KJMA fit is very effective to highlight the contrasting behaviour of LP1 and Q-05 when their annealing behaviour is compared at nearly the same temperature. While both samples can be modelled using the Höfler and Averback equation, only Q-05 can be also described by a blocked growth model.

Table 1. Goodness of fit of isothermal curves regressions: adjusted R-square (R^2) and reduced chi-square (χ^2) indexes for LP1 and Q-05 samples. Each equation is explained in the theoretical background section.

	T (°C)	**Burke-gen.** (eq. 3 with n = 10)		**Höfler & Averback** (eq. 4)			**Michels** (eq. 6)		**KJMA** (eq. 7)	
		R^2	R^2	R^2	χ^2	m	R^2	χ^2	R^2	χ^2
LP1	375	0.86	9.24	0.92	5.10	0.22	0.92	5.14	0.95	3.10
	425	0.84	9.13	0.98	1.38	0.18	0.79	12.27	0.92	4.71
	475	0.96	3.93	0.97	3.06	0.23	0.73	24.43	0.89	9.72
Q-05	500	-0.95	7.18	0.90	0.38	0.16	0.86	0.51	0.93	3.02
	550	-0.43	9.72	0.97	0.22	0.13	0.93	0.45	0.94	0.40
	600	0.18	9.65	0.99	0.13	0.20	0.89	1.32	0.97	0.39

Determining the growth kinetics. In order to carry on the kinetic analysis of nanocrystal growth of LP1 and Q-05 on a similar basis, the rate parameters K obtained for both samples from the Höfler and Averback fits of the three isotherms are considered. The determination of the crystallite growth apparent activation energy is then calculated by means of the Arrhenius equation:[46]

$$K = K_0 \exp\left(\frac{E_a}{RT}\right) \quad (7)$$

where K is the rate constant, E_a the activation energy for isothermal grain growth, R the universal gas constant, T the absolute temperature of each isotherm, and K_0 a pre-factor constant (which is usually ignored, having a negligible temperature dependence). [38,45,46,49]

Figure 5 shows the results of direct fitting of K data points by equation 7 as implemented in the OriginPro v.8 analysis software. The apparent activation energy E_a calculated for both samples is identical within the standard deviation: 26.4(2) and 26.9(8) kJ·mol^{-1} for LP1 and Q-05, respectively.

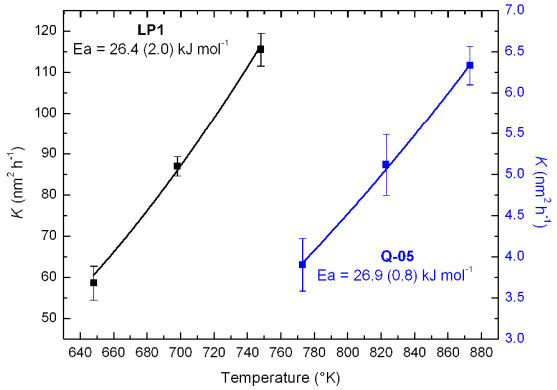

Figure 5. Apparent activation energy of crystallite growth (E_a) for LP1 and Q-05 by the Arrhenius plot (solid lines).

DISCUSSION

The experimental and modelling work reported in the previous sections suggests that the kinetics governing the coarsening stage at the intermediate times of the isothermal annealing process are similar for both the nanocrystalline anatase samples here studied, in spite of the differences in the solvent and catalyst used for the synthesis (i.e. benzyl alcohol and acetic acid for LP1, isobutyl acetate and hydrochloric acid for Q-05). However, a completely different behaviour is observed at the longer annealing times during which the LP1 sample shows a steady and persistent coarsening whereas Q-05 undergoes a growth blocking. In order to understand the origin of the limited growth or size "lock-up" phenomenon at long times for Q-05, several factors discussed in the literature can be invoked: i) sample surface (thickness effect), ii) grain-boundary pinning by second-phase particles (Zener drag), iii) pores (pore drag), and iv) impurities (solute drag).

The first effect here considered is the so called "thickness effect" that is usually active when a sample is deposited as a thin film. It takes place when the constituting-film crystallites with different initial crystal size upon coarsening reach a diameter which is similar to the film thickness.[42,63,64] Since the sample layer within the crucibles are much thicker than their crystallite size (some millimetres against a few nanometres), the thickness effect can be ruled out as possible cause for the Q-05 grain growth locking.

Other reported phenomena hampering the thermally activated grain growth of a crystalline phase are related to the locking of the grain boundaries migration due to the occurrence of small particles of a second phases (i.e. the so called "Zener drag" phenomenon) or the presence of pores (pore drag).[31,65–68] It is important to remind here that each grain growth mechanism has a characteristic activation energy range: typically, E_a(*grain-boundary migration*) > E_a(*grain-boundary diffusion*) > E_a(*surface diffusion*).[31,68–70] Knauth and Auer reported an activation energy of about 100 kJ·mol^{-1} for the grain boundary migration process responsible for the growth of anatase nanoparticles.[71] Since the activation energy calculated for LP1 and Q-05 samples in our study is less than 27 kJ·mol^{-1}, it is unlikely that the grain boundary migration mechanism is active in the ranges of temperature treatment of LP1 and Q-05 considered here. Although it has been reported that the grain growth of anatase nanoparticles can be influenced by the presence of open pores even in the second stage of sintering,[68,72,73] the pore pinning effect usually takes place in pressed samples at the third (final) stage of sintering when the investigated powder reaches a density greater than 90%; this is a level of sintering which is never reached by our loose powders. As far the effect of impurity phases, no

phases other than anatase are detected by XRD in our hea t treated samples, therefore a Zener drag process acting on Q-05 could be discarded.

In light of the above, it seems reasonable to suppose that, the "lock-up" phenomenon acting on the sample Q-05 could be related to the different chemical environment during the synthesis of nanoanatase powders of this sample compared to LP1 sample.

It is well known that the anatase doping by means of molecules or ions can inhibit or speed up the grain growth mechanisms.[74–77] Hence, the isobutyl acetate ($C_6H_{12}O_2$) or the hydrochloric acid (HCl) (or one of their constituting ions) used as solvent and catalyst for preparation of sample Q-05 can be chemisorbed on the surface of anatase nanocrystals.

Chemisorbed isobutyl acetate can be ruled out as a possible cause for the pinning effect because its self ignition point (~422 °C) is well below the lowest annealing temperature of sample Q-05 (500 °C). Indeed the TG/DTA curve of sample Q-05 shows a strong combustion reaction at about 430°C which is likely due to the complete removal of isobutyl acetate from the anatase powders.

The other two possible dopants, with some possible influence on the grain growth process of sample Q-05, are carbon and chlorine ions deriving from tetraisopropoxide (*TTIP*–$Ti(OC_3H_7)_4$) precursor or acetic acid and from hydrochloric acid, respectively.

Inspired by the work of Chen et al.,[74] Eder and Windle suggested that carbon impurities may inhibit the growth of anatase nanoparticles by reducing the surface energy.[75] A similar effect was also documented during the growth of aluminium nanoparticles.[78] From these works, it emerges that an oxidative atmosphere (air) promotes the crystal growth by removing the carbon particles, whereas under reducing atmosphere (e.g. argon or nitrogen) carbon is retained by the crystal surface producing a "lock up" effect. Since the TG/DTA analysis performed under oxidative (air) and reducing (nitrogen) atmospheres marginally affect the crystal growth of the Q-05 powder (i.e. the maximum Q-05 crystal size at 900 °C is ~9.5 nm), the presence of carbon as impurity on the anatase surface and, therefore, its contribution as locking agent during the sintering treatments, can be excluded.

Hence, the focus on a possible agent limiting the crystal growth of nano-TiO_2 must be directed to the presence of chlorine as an impurity in the sample Q-05. As well as chlorine, it has been demonstrated that other anions (such as phosphate groups) have an inhibitory effect on the crystal grain growth of nanosized titania during high temperature treatments.[76]

Although the effects of HCl and the Cl^- ion on anatase nanopowders were object of many studies in the literature,[77,79–87] their implication in the growth processes has not been fully clarified yet. As emphasized by Hanaor and Sorrell in a recent review on the anatase to rutile phase transformation, the anionic doping of chlorine in the anatase lattice is constrained by both size and charge mismatch between chlorine and oxygen anions.[77] Furthermore, two conflicting behaviours can be identified. In fact, chlorine can either inhibit,[83,85,86] or promote,[82,84,87] the phase transition from anatase to rutile (A→R), and therefore has a deterrent effect on the grain growth rather than the reverse. In fact it is well known that (rutile becomes thermodynamically favoured over anatase above a given nanocrystal size).[88,89]

Reconsidering these previous studies in line with Wu et al.,[81] the crystal growth evolution and the subsequent polymorphic A→R transformation of TiO_2 powders can be rationalized by taking into account the interplay between the initial crystallite sizes and the HCl concentration, associated to the temperature of the thermal treatment. Indeed, higher HCl concentrations favour the anatase to rutile transformation by reducing the transition temperature and promoting larger TiO_2 particles.[82,84,87] On the other hand, the A→R transformation is strongly inhibited (and the anatase crystal growth as well) when TiO_2 nanocrystals are synthesized in the presence of HCl at low concentrations, and their average grain size prior to the thermal treatment is extremely small.[83,85,86]

This last case seems to perfectly describe the thermal evolution of the sample Q-05. The extremely small grain size (~5 nm), and the low HCl concentration during the synthesis process,[56] suggest that a very small amount of chlorine ions is chemisorbed on the anatase surface, inducing the previously described "lock-up" phenomenon. We are dealing with reagents molar ratios that are 1.05/0.1

(isobutyl acetate/TTIP) and 0.0072/0.1 (HCl/TTIP). As a consequence, an enhanced stability of the anatase polymorph up to 900 °C (just ~10% of the A→R transformation occurred at this temperature) is observed.

CONCLUSIONS

Two nano-anatase powders, labelled as LP1 and Q-05, have been synthesized starting from a common precursor, titanium tetraisopropoxide, by reflux at temperature characteristics of the different organic solvents (benzyl alcohol for LP1 and isobutyl acetate for Q-05). Another critical difference in the synthesis was the use of acetic acid for LP1 and hydrochloric acid for Q-05. Apart the different solvents and acids, both samples underwent the same processing (i.e. spray drying of as-synthesized suspensions). Monitoring the thermal treatment of these powders at different isotherms showed a very limited crystals growth after long annealing times for Q-05, while LP1 exhibited a continuous crystallite coarsening. In agreement with the literature,[51,52] we found that the grain growth kinetics of both nanoanatase samples can be fitted by the Höfler and Averback equation.[50] However, only the sample Q-05 can be also satisfactorily modelled by an expression entailing a limiting growth factor (i.e. the KJMA equation),[53] while fitting the annealing curve of LP1 at nearly the same temperature with this expression yielded physically-unreasonable results. The apparent activation energy of crystallite growth is identical (on average ~27 $kJ \cdot mol^{-1}$) for both samples. This value of E_a falls in the range comprised between 15 and 30 $kJ \cdot mol^{-1}$, identified as the energetic field required for the formation of ionized molecules when crystal growth processes are assisted by proton-transfer.[52,90–92]

It can be inferred that the lock up phenomenon occurring in Q-05 is due to the presence of chlorine chemisorbed at the anatase surface. The use of different acids for the synthesis of LP1 and Q-05 therefore played a key role in the contrasting crystals growth behaviour upon heat treatment of the two investigated nanoanatase powders.

The slow grain growth of anatase also brought about a slowing down of the anatase to rutile transition. The inhibition of this phase transformation can depend on thermodynamic reasons related to the size of the crystallites (indirect control by chlorine)[88,89] as well as through a locking of the nucleation (no phase transition) on surface or interface of crystals.[93] Indeed, dopants on anatase surface can stabilize the low temperature phase by raising the activation energy of the phase transition compared to powders without doping.[74,94]

The limited crystal growth of the spray-dried nanoanatase powders synthesized by reflux method in the presence of HCl (i.e. sample Q-05 here) makes this material particularly suitable to be used in all kinds of application where, despite a heat treatment, the anatase particles have to maintain a small size, then a high specific surface area, as the electrode in DSSC devices.

Although the accumulation of chlorine on the surface of TiO_2, as well as CeO_2, produces a decreasing in the catalytic activity of these materials,[95–97] and therefore could be present when nanoanatase is applied for the engineering of DSSC electrodes, it has been demonstrated that this effect can be overcome by means of a water washing.[95]

TiO_2 electrodes in DSSC require that both the anatase phase and a large surface area of the porous oxide layer are preserved during the thermal treatments which are typically applied to the devices. Nanoanatase powders Q-05 perfectly fulfil both these requirements.

AUTHOR INFORMATION

Corresponding author

*E-mail: cru@unife.it. Phone: +39-0532-974731. Fax: +39-0532-974617.

Notes

The authors declare no competing financial interest.

ACKNOWLEDGEMENTS

This work was supported by the project "Nanomaterials for energy" funded under the framework agreement program of the Italian Ministry of Economic Development (MiSE), the National Institute of Foreign Commerce (ICE), and the Conference of Italian University Rectors (CRUI).

One of the authors (D.C.) would like to thank Dr. Alessandro di Bona of C.N.R. – Istituto Nanoscienze for useful discussion on this paper.

This work is done in partial fulfilment of the requirements for the Doctor Degree of D. C.

REFERENCES

(1) Hoffmann, M. R.; Martin, S. T.; Choi, W.; Bahnemann, D. W. *Chem. Rev.* **1995**, *95*, 69–96.
(2) Shao, W.; Nabb, D.; Renevier, N.; Sherrington, I.; Fu, Y.; Luo, J. *J. Electrochem. Soc.* **2012**, *159*, D671–D676.
(3) Kintaichi, Y.; Hamada, H.; Tabata, M.; Sasaki, M.; Ito, T. *Catal. Lett.* **1990**, *6*, 239–244.
(4) Maldotti, A.; Molinari, A.; Amadelli, R. *Chem. Rev.* **2002**, *102*, 3811–3836.
(5) Johnson, R. W.; Thiele, E. S.; French, R. H. *Tappi J.* **1997**, *80*, 233–239.
(6) Weir, A.; Westerhoff, P.; Fabricius, L.; Hristovski, K.; von Goetz, N. *Environ. Sci. Technol.* **2012**, *46*, 2242–2250.
(7) Fujishima, A.; Rao, T. N.; Tryk, D. A. *J. Photochem. Photobiol. C Photochem. Rev.* **2000**, *1*, 1–21.
(8) Traversa, E.; Vona, M. L. D.; Licoccia, S.; Sacerdoti, M.; Carotta, M. C.; Crema, L.; Martinelli, G. *J. Sol-Gel Sci. Technol.* **2001**, *22*, 167–179.
(9) Chen, H.-Y.; Kuang, D.-B.; Su, C.-Y. *J. Mater. Chem.* **2012**, *22*, 15475–15489.
(10) O'Regan, B.; Grätzel, M. *Nature* **1991**, *353*, 737–740.
(11) Grätzel, M. *Inorg. Chem.* **2005**, *44*, 6841–6851.
(12) Kalowekamo, J.; Baker, E. *Sol. Energy* **2009**, *83*, 1224–1231.
(13) Yoon, S.; Tak, S.; Kim, J.; Jun, Y.; Kang, K.; Park, J. *Build. Environ.* **2011**, *46*, 1899–1904.
(14) Singh, P. K.; Bhattacharya, B.; Nagarale, R. K.; Pandey, S. P.; Kim, K.-W.; Rhee, H.-W. *Synth. Met.* **2010**, *160*, 950–954.
(15) Lee, H.-S.; Bae, S.-H.; Jo, Y.; Kim, K.-J.; Jun, Y.; Han, C.-H. *Electrochimica Acta* **2010**, *55*, 7159–7165.
(16) Liu, X.; Zhang, W.; Uchida, S.; Cai, L.; Liu, B.; Ramakrishna, S. *Adv. Mater.* **2010**, *22*, E150–E155.
(17) Zhang, C.-R.; Liu, Z.-J.; Chen, Y.-H.; Chen, H.-S.; Wu, Y.-Z.; Feng, W.; Wang, D.-B. *Curr. Appl. Phys.* **2010**, *10*, 77–83.
(18) Dürr, M.; Bamedi, A.; Yasuda, A.; Nelles, G. *Appl. Phys. Lett.* **2004**, *84*, 3397–3399.
(19) Liska, P.; Thampi, K. R.; Grätzel, M.; Brémaud, D.; Rudmann, D.; Upadhyaya, H. M.; Tiwari, A. N. *Appl. Phys. Lett.* **2006**, *88*, 203103.
(20) Barbé, C. J.; Arendse, F.; Comte, P.; Jirousek, M.; Lenzmann, F.; Shklover, V.; Grätzel, M. *J. Am. Ceram. Soc.* **1997**, *80*, 3157–3171.
(21) Colodrero, S.; Mihi, A.; Häggman, L.; Ocaña, M.; Boschloo, G.; Hagfeldt, A.; Míguez, H. *Adv. Mater.* **2009**, *21*, 764–770.
(22) Laskova, B.; Zukalova, M.; Kavan, L.; Chou, A.; Liska, P.; Wei, Z.; Bin, L.; Kubat, P.; Ghadiri, E.; Moser, J. E.; Grätzel, M. *J. Solid State Electrochem.* **2012**, *16*, 2993–3001.
(23) Antonietta Loi, M.; Hummelen, J. C. *Nat. Mater.* **2013**, *12*, 1087–1089.
(24) Boix, P. P.; Nonomura, K.; Mathews, N.; Mhaisalkar, S. G. *Mater. Today* 2014, *17*, 16–23.
(25) Ramasamy, E.; Lee, W. J.; Lee, D. Y.; Song, J. S. *J. Power Sources* **2007**, *165*, 446–449.
(26) Ito, S.; Chen, P.; Comte, P.; Nazeeruddin, M. K.; Liska, P.; Péchy, P.; Grätzel, M. *Prog. Photovolt. Res. Appl.* **2007**, *15*, 603–612.
(27) Chen, D.; Huang, F.; Cheng, Y.-B.; Caruso, R. A. *Adv. Mater.* **2009**, *21*, 2206–2210.

(28) Kang, S.-J. L. *Sintering: Densification, Grain Growth and Microstructure*; 1st ed.; Butterworth-Heinemann, 2004.
(29) Fang, Z. Z.; Wang, H. *Int. Mater. Rev.* **2008**, *53*, 326–352.
(30) Jeong, N. C.; Farha, O. K.; Hupp, J. T. *Langmuir* **2011**, *27*, 1996–1999.
(31) Sierra, E. J. *Sintering, Grain Growth, and Electrical Conductivity of Cobalt Oxide Doped* $Ce_{1-x}Gd_xO_{2-x/2}$; 2005.
(32) Lange, F. F. *J. Am. Ceram. Soc.* **1984**, *67*, 83–89.
(33) Mayo, M. J.; Hague, D. C.; Chen, D.-J. *Mater. Sci. Eng. A* **1993**, *166*, 145–159.
(34) Gribb, A. A.; Banfield, J. F. *Am. Mineral.* **1997**, *82*, 717–728.
(35) Gao, Y.; Elder, S. A. *Mater. Lett.* **2000**, *44*, 228–232.
(36) Kingery, W. D.; Francois, B. *Pp 471-498 Sinter. Relat. Phenom. Proc. Int. Conf. Univ Notre Dame Kuczynski G C Hooton N Gibbon C F Eds N. Y. Gordon Breach* 1968.
(37) Lange, F. F.; Kellett, B. J. *J. Am. Ceram. Soc.* **1989**, *72*, 735–741.
(38) Liu, K. W.; Mücklich, F. *Acta Mater.* **2001**, *49*, 395–403.
(39) Burke, J. E. *Trans. Am. Inst. Min. Metall. Eng.* **1949**, *180*, 73–91.
(40) Atkinson, H. V. *Acta Metall.* **1988**, *36*, 469–491.
(41) German, R. M. *Sintering Theory and Practice*; Wiley-Interscience: New York, 1996.
(42) Beck, P. A.; Kremer, J. C.; Demer, L. J.; Holzworth, M. L. *Trans AIME* **1948**, *175*, 372–400.
(43) Burke, J. E.; Turnbull, D. *Prog. Met. Phys.* **1952**, *3*, 220–292.
(44) Vandermeer, R. A.; Hu, H. *Acta Metall. Mater.* **1994**, *42*, 3071–3075.
(45) Malow, T. R.; Koch, C. C. *Acta Mater.* **1997**, *45*, 2177–2186.
(46) Michels, A.; Krill, C. E.; Ehrhardt, H.; Birringer, R.; Wu, D. T. *Acta Mater.* **1999**, *47*, 2143–2152.
(47) Natter, H.; Schmelzer, M.; Löffler, M.-S.; Krill, C. E.; Fitch, A.; Hempelmann, R. *J. Phys. Chem. B* **2000**, *104*, 2467–2476.
(48) Rollett, A.; Humphreys, F. J.; Rohrer, G. S.; Hatherly, M. *Recrystallization and Related Annealing Phenomena*; Elsevier, 2004.
(49) Kirsch, B. L.; Richman, E. K.; Riley, A. E.; Tolbert, S. H. *J. Phys. Chem. B* **2004**, *108*, 12698–12706.
(50) Höfler, H. J.; Averback, R. S. *Scr. Metall. Mater.* **1990**, *24*, 2401–2406.
(51) Liu, He-Zhou; Hu, Wen-Bin; Gu, Ming-Yuan; Wu, Ren-Jie. *J. Inorg. Mater.* **2002**, *17*, 429–436.
(52) Li, G.; Li, L.; Boerio-Goates, J.; Woodfield, B. F. *J. Am. Chem. Soc.* **2005**, *127*, 8659–8666.
(53) Wang, F.; Richards, V. N.; Shields, S. P.; Buhro, W. E. *Chem. Mater.* **2014**, *26*, 5–21.
(54) Christian, J. W. *The Theory of Transformations in Metals and Alloys* (Part I + II); Newnes, 2002.
(55) Ciccarella, G.; Cingolani, R.; De Marco, L.; Gigli, G.; Melcarne, G.; Martina, F.; Matteucci, F.; Spadavecchia, J. *Process for the preparation of titanium dioxide with nanometric dimensions and controlled shape*. WO 2009/101640 A1, August 20, 2009.
(56) Zama, I.; Matteucci, F.; Martelli, C.; Ciccarella, G. *Process for the preparation of titanium dioxide having nanometric dimensions and controlled shape*. WO 2011/006659 A1, January 20, 2011.
(57) Bruker AXS. *TOPAS 4-1 User Manual*; Bruker AXS GmbH, Karlsruhe, Germany.
(58) Cheary, R. W.; Coelho, A. *J. Appl. Crystallogr.* **1992**, *25*, 109–121.
(59) Cheary, R. W.; Coelho, A.; Cline, J. P. *J. Res. Natl. Inst. Stand. Technol.* **2004**, *109*, 1–25.
(60) Kern, A.; Coelho, A. A.; Cheary, R. W. In *Diffraction Analysis of the Microstructure of Materials*; Mittemeijer, P.; Scardi, P., Eds.; Springer Series in Materials Science; Springer Berlin Heidelberg, 2004; pp. 17–50.
(61) Balzar, D. In *Microstructure analysis from diffraction*; R. L. Snyder, H. J. Bunge, and J. Fiala, 1999.

(62) OriginLab Corporation. *OriginLab V-8 User Guide*; OriginLab Corporation One Roundhouse Plaza Northampton, MA 01060 USA.
(63) Yu, J.; Zhao, X.; Zhao, Q. *J. Mater. Sci. Lett.* **2000**, *19*, 1015–1017.
(64) An, Z.; Ding, H.; Meng, Q.; Rong, Y. *Scr. Mater.* **2009**, *61*, 1012–1015.
(65) Hunderi, O.; Ryum, N. *Acta Metall.* **1982**, *30*, 739–742.
(66) Nes, E.; Ryum, N.; Hunderi, O. *Acta Metall.* **1985**, *33*, 11–22.
(67) Li, W.-B.; Easterling, K. E. *Acta Metall. Mater.* **1990**, *38*, 1045–1052.
(68) Li, J.; Ye, Y. *J. Am. Ceram. Soc.* **2006**, *89*, 139–143.
(69) Wang, J.; Raj, R. *J. Am. Ceram. Soc.* **1990**, *73*, 1172–1175.
(70) Chen, I.-W.; Wang, X.-H. *Nature* **2000**, *404*, 168–171.
(71) Knauth, P.; Auer, G. *Solid State Ion.* **2002**, *147*, 115–121.
(72) Mayo, M. J.; Hague, D. C. *Nanostructured Mater.* **1993**, *3*, 43–52.
(73) Skandan, G.; Hahn, H.; Roddy, M.; Cannon, W. R. *J. Am. Ceram. Soc.* **1994**, *77*, 1706–1710.
(74) Chen, B.; Zhang, H.; Gilbert, B.; Banfield, J. F. *Phys. Rev. Lett.* **2007**, *98*, 106103.
(75) Eder, D.; Windle, A. H. *Adv. Mater.* **2008**, *20*, 1787–1793.
(76) Feng, X.; Liu, J.; Li, P.; Zhang, Y.; Wei, Y. *Rare Metals* **2009**, *28*, 385–390.
(77) Hanaor, D. A. H.; Sorrell, C. C. *J. Mater. Sci.* **2011**, *46*, 855–874.
(78) De Castro, C. L.; Mitchell, B. S. *Mater. Sci. Eng. A* **2005**, *396*, 124–128.
(79) Knoll, H.; Kühnhold, U. *Naturwissenschaften* **1957**, *44*, 394–394.
(80) Rao, C. N. R.; Turner, A.; Honig, J. M. *J. Phys. Chem. Solids* **1959**, *11*, 173–175.
(81) Wu, M.; Lin, G.; Chen, D.; Wang, G.; He, D.; Feng, S.; Xu, R. *Chem. Mater.* **2002**, *14*, 1974–1980.
(82) Readey, M. J.; Readey, D. W. *J. Am. Ceram. Soc.* **1987**, *70*, C358–C361.
(83) Takahashi, Y.; Matsuoka, Y. *J. Mater. Sci.* **1988**, *23*, 2259–2266.
(84) Gennari, F. C.; Pasquevich, D. M. *J. Am. Ceram. Soc.* **1999**, *82*, 1915–1921.
(85) Wang, C.-C.; Ying, J. Y. *Chem. Mater.* **1999**, *11*, 3113–3120.
(86) Song, K. C.; Pratsinis, S. E. *J. Am. Ceram. Soc.* **2001**, *84*, 92–98.
(87) Long, M.; Cai, W.; Chen, H.; Xu, J. *Front. Chem. China* **2007**, *2*, 278–282.
(88) Zhang, H.; Banfield, J. F. *J. Mater. Chem.* **1998**, *8*, 2073–2076.
(89) Barnard, A. S.; Curtiss, L. A. *Nano Lett.* **2005**, *5*, 1261–1266.
(90) Collier, W. B.; Ritzhaupt, G.; Devlin, J. P. *J. Phys. Chem.* **1984**, *88*, 363–368.
(91) Fernández-García, M.; Wang, X.; Belver, C.; Hanson, J. C.; Rodriguez, J. A. *J. Phys. Chem. C* **2007**, *111*, 674–682.
(92) Vives, S.; Meunier, C. *Powder Diffr.* **2009**, *24*, 205–220.
(93) Zhang, H.; Banfield, J. F. *Am. Mineral.* **1999**, *84*, 528–535.
(94) Banfield, J. F.; Bischoff, B. L.; Anderson, M. A. *Chem. Geol.* **1993**, *110*, 211–231.
(95) Yamazaki, S.; Yoshida, A.; Abe, H. *J. Photoch. Photobio. A* **2005**, *169*, 191–196.
(96) Kondarides, D. I.; Zhang, Z.; Verykios, X. E. *J. Catal.* **1998**, *176*, 536–544.
(97) Huang, Y.; Wang, A.; Li, L.; Wang, X.; Zhang, T. *Catal. Commun*. **2010**, *11*, 1090–1093.

Tables

Table 1. Goodness of fit of isothermal curves regressions: adjusted R-square (R^2) and reduced chi-square (χ^2) indexes for LP1 and Q-05 samples. Each equation is explained in the theoretical background section.

	T (°C)	**Burke-gen.** (eq. 3 with n = 10)		**Höfler & Averback** (eq. 4)			**Michels** (eq. 6)		**KJMA** (eq. 7)	
		R^2	R^2	R^2	χ^2	m	R^2	χ^2	R^2	χ^2
LP1	375	0.86	9.24	0.92	5.10	0.22	0.92	5.14	0.95	3.10
	425	0.84	9.13	0.98	1.38	0.18	0.79	12.27	0.92	4.71
	475	0.96	3.93	0.97	3.06	0.23	0.73	24.43	0.89	9.72
Q-05	500	-0.95	7.18	0.90	0.38	0.16	0.86	0.51	0.93	3.02
	550	-0.43	9.72	0.97	0.22	0.13	0.93	0.45	0.94	0.40
	600	0.18	9.65	0.99	0.13	0.20	0.89	1.32	0.97	0.39

Captions for Figures

Figure 1. TG (left axis, black lines) and DTA (right axis, blue lines) analysis of samples LP1 (on the left) and Q-05 (on the right). Solid and dashed lines represent air and nitrogen atmospheres, respectively.

Figure 2. LP1 and Q-05 crystallite growth vs. isothermal annealing time. Error bars, where not shown, are within the symbol size. Lines are guide to the eye (with temperature in °C).

Figure 3. Mean crystallite size *vs.* isothermal annealing time (LP1 and Q-05 on the left and on the right side, respectively). Comparison of curve fittings by means of two different equations of growth: Höfler and Averback (*solid lines*)[50] and Burke (generalized parabolic grain growth model)[46] with grain growth exponent $n = 10$ (*dashes*).

Figure 4. Isothermal annealing curves for LP1 at 475°C (*left*) and Q-05 at 500°C (*right*). Comparison of curve fittings by means of three different equations of growth: Höfler and Averback (*solid lines*),[50] Michels (*dotted line*),[46] and KJMA (*dash-dot line*).

Figure 5. Apparent activation energy of crystallite growth (E_a) for LP1 and Q-05 by the Arrhenius plot (solid lines).

For Table of Contents Use Only

Limited Crystallite Growth upon Isothermal Annealing of Nanocrystalline Anatase

Davide Casotti,[a,b] Matteo Ardit,[a] Robert Dinnebier,[c] Michele Dondi,[d] Francesco Matteucci,[e] Isabella Zama,[f] and Giuseppe Cruciani,[*,a]

[a] Department of Physics and Earth Sciences, University of Ferrara, Italy
[b] Department of Physics, Informatics and Mathematics, University of Modena and Reggio Emilia, Modena, Italy
[c] Max-Plank Institute for Solid State Research, Stuttgart, Germany
[d] Institute of Science and Technology for Ceramics, CNR-ISTEC Faenza, Italy
[e] Nanotechnology Living Lab (NTLL) at Dhitech, Lecce, Italy
[f] Tozzi Renewable Energy, Ravenna, Italy

TOC graphics

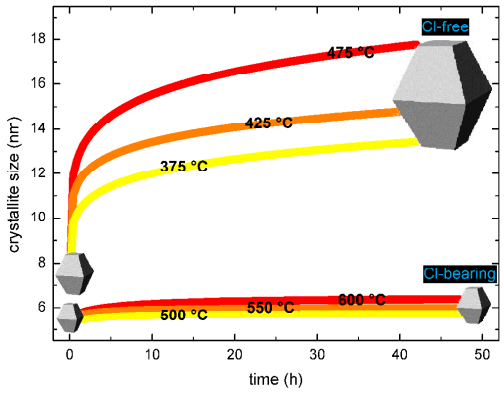

TOC synopsis

Nanotitania with stable anatase phase and crystal size growth limited to about 6 nm maximum upon annealing up to 900°C was achieved by reflux synthesis of organic solvents in the presence of hydrochloric acid. Extensive modelling of crystal growth kinetics supports the occurrence of a size locking phenomena ascribable to the effects of chlorine ions adsorbed on the anatase grain.